Environmental Science Nano

"Switching on" iron in clay minerals

Journal:	*Environmental Science: Nano*
Manuscript ID	EN-ART-02-2019-000228.R2
Article Type:	Paper
Date Submitted by the Author:	29-Apr-2019
Complete List of Authors:	Ilgen, Anastasia ; Sandia National Laboratories, Geochemistry Department Kukkadapu, Ravi; Pacific Northwest National Laboratory, Leung, Kevin; Sandia National Laboratories, Surface and Interface Science Washington, Rachel; Sandia National Laboratories

“Switching on” iron in clay minerals

A.G. Ilgen,[1]* R.K Kukkadapu,[2] K. Leung,[3] and R.E. Washington[1]

1. Sandia National Laboratories, Geochemistry Department, PO Box 5800 Mailstop 0754, Albuquerque, NM 87185-0754, United States
2. Pacific Northwest National Laboratory, Environmental Molecular Sciences Laboratory, Richland, WA, United States
3. Sandia National Laboratories, Computation Materials and Data Science Department, PO Box 5800 Mailstop 1415, Albuquerque, NM 87185-1415, United States

*Corresponding author. E-mail agilgen@sandia.gov

Environmental Significance statement

The reactivity of iron (Fe), its redox cycling, and complexation reactions on iron-containing mineral surfaces govern fate and transport of chemical species in the environment. Nano- to micron-sized clay mineral particles can contain iron either in their crystalline structure, or adsorbed on their surfaces. The reactivity of the iron species associated with these nano-scale natural particles is largely unknown. We discovered the mechanism by which iron residing in clay mineral structures becomes redox-active under oxygen-free conditions. We demonstrate that Fe(II)-O-Fe(III)-containing moieties at clay mineral edge sites participate in electron transfer, and lower energetic cost of water desorption from these sites increases the kinetics of redox reactions. This mechanism helps explaining trends observed for redox-sensitive nutrients and contaminants in the environment.

“Switching on” iron in clay minerals

A.G. Ilgen,[1]* R.K Kukkadapu,[2] K. Leung,[1] and R.E. Washington[1]

1. Sandia National Laboratories, Geochemistry Department, PO Box 5800 Mailstop 0754, Albuquerque, NM 87185-0754, United States
2. Pacific Northwest National Laboratory, Environmental Molecular Sciences Laboratory, Richland, WA, United States

*Corresponding author. E-mail agilgen@sandia.gov

Abstract

Being the fourth most abundant element in the Earth's crust, iron (Fe) is a key player in myriad biogeochemical processes. Iron that resides in the structures of nano- to micron-scale clay mineral particles undergoes cycling between Fe(II) and Fe(III). This iron comprises a large redox-active pool in surface environments, controlling the fate and transport of nutrients and contaminants. The mechanism of electron transfer involving this iron species is poorly understood. We observe that Fe(III) in clay minerals does not oxidize arsenic As(III), unless a minor amount of Fe(II) is introduced into the predominantly-Fe(III) structure. These "activated" clay minerals are redox-active both in the presence and absence of oxygen. In the presence of oxygen, Fe(II) catalyzes the production of reactive oxygen species; however, the oxidation pathway in the absence of oxygen is unknown. Here we show that under oxygen-free conditions, the redox-active species in clay minerals is Fe^{II}-O-Fe^{III} moieties at the edge sites. We used *in situ* and *ex situ* spectroscopic methods, including X-ray absorption, Mössbauer, and diffuse reflectance spectroscopies, as well as *ab initio* calculations. Our *ab initio* calculations show that desorption of water from an Fe^{II}-O-Fe^{III} site in clay mineral requires less energy, compared to a fully-oxidized Fe^{III}-O-Fe^{III} site. We propose that this lower barrier for the desorption of water increases the apparent kinetics of redox reactions on clay mineral surfaces.

Introduction

Iron (Fe) is the fourth most abundant element in the Earth's crust and is frequently found in the structures of clay minerals. Clay minerals are fine-crystalline solids, with the average particle size ranging from nanometers to microns.[1] Due to the large reactive surface areas, redox reactions on clay mineral surfaces control the transport, bioavailability, and degradation of redox-sensitive nutrients and contaminants in surface environments.[2] Iron can comprise up to 30 wt.% of a clay mineral,[2] and can reside in either the tetrahedral (substituting for silicon) or in the octahedral (substituting for aluminum) lattice sites[2] (Figure 1). In the octahedral site, Fe can be in either +2 or +3 oxidation states.[2, 3] The octahedral Fe(II) can reduce pollutants, such as nitro-aromatic compounds,[4] technetium, [5, 6] uranium, [5] and chromium.[7] The oxidation of pollutants, such as arsenic and antimony, on the surfaces of Fe(III)-rich clay minerals under both oxygenated and oxygen-free conditions was first reported in 2012.[8] For the oxidation to take place, less than one fifth of the Fe(III) residing in the octahedral sheet has to be reduced to Fe(II), and the tri-octahedral moiety containing Fe(II)-Fe(III)-Fe(III) was proposed as the reactive species.[8] Since then, scientists have discovered that in the presence of oxygen, Fe(II) in clay mineral structures catalyzes the production of reactive oxygen species (e.g., hydroxyl radicals), which is the proposed oxidant under oxygenated conditions.[9, 10] However, the reactive moieties and chemical mechanism by which Fe(III)-rich clay minerals oxidize chemical species under oxygen-free conditions, and the reasons why some amount of Fe(II) is required for this reaction to proceed, remained unknown.

Here we propose a new mechanistic explanation for the observed oxidation on the surfaces of clay minerals with both Fe(II) and Fe(III) residing in their structure. We use element-specific

spectroscopic tools to quantify—both *in situ* and *ex situ*—the local chemical environment and transformations of the reactive moieties in natural Fe-rich clay mineral nontronite (NAu-1 standard mineral). We show that by introducing Fe(II) either into clay mineral structure, or at the clay mineral edges, Fe(III) in the clay mineral becomes reactive, or "switched on".

We used *in situ* technique—diffuse reflectance spectroscopy—to track the changes in the solid-phase-speciation of iron as a function of reaction with arsenic. This technique is sensitive to the Fe(II)↔Fe(III) intervalence charge-transfer band, which can be monitored in liquid in suspensions containing clay minerals.[11] The *ex situ* characterization techniques used in this study are X-ray absorption (XAS)[12-15] and Mössbauer spectroscopies.[16-18] The combination of these element-specific techniques allows for quantifying the exact chemical environment and oxidation state of different iron species in crystalline and amorphous phases.

Figure 1.

Figure 1. Structure of nontronite. The octahedral sheet is labeled "O" and the tetrahedral sheets are labeled "T". Iron in the octahedral sites is coordinated to six oxygens and can be in either +2 or +3 oxidation states. Adsorption of arsenic, tested here, takes place at the edge sites.

Experiments examining redox reactions on clay mineral surfaces and the pathways by which electrons can be transferred from Fe(II) to Fe(III) within the octahedral sheet have been routinely conducted using natural Fe-rich clay minerals (mostly nontronites).[3, 19-27] Recent work highlights that the same reactivity trends hold for synthetic nontronites; namely that the mineral surface is capable of oxidizing pollutants under oxygenated and oxygen-free conditions, when both Fe(II) and Fe(III) are present in the octahedral sheet, or at the edge sites of clay mineral.[15, 28] Understanding chemical mechanisms controlling the reactivity of the Fe(II)/Fe(III) redox couple

in nano-scale clay mineral particles can inspire the development of novel reactive sorbent and membrane materials, mixed-oxidation state catalytic substrates,[29] and allows for accurate predictions of environmental behaviors of redox-sensitive chemical species.

Methods

Mineral substrates

The natural nontronite NAu-1, with Fe content of 24.2 wt.%, was purchased from the Source Clays Repository of the Clay Minerals Society. Nontronite NAu-1 was fractionated to < 2 μm particle size, washed in a 1 M ammonium acetate-acetic acid buffer (pH 5.0±0.1) to remove carbonates, and saturated with Na^+. The surface area of nontronite NAu-1 was 46.5 m^2 g^{-1}, as reported earlier.[15] The partial reduction, or activation, treatment was performed using citrate-bicarbonate-dithionite (CBD) procedure described elsewhere.[30] To start the activation, 50 mg of sodium dithionite $Na_2S_2O_4$ was added per each 100 mg of nontronite, suspended in a citrate-bicarbonate buffer, and allowed to react for 30 minutes at 70°C temperature. This treatment was carried out in an anoxic (96% N_2 and 4% H_2 mixture) glove box equipped with a palladium oxygen-scrubbing catalyst and oxygen O_2(g) sensor with the detection limit of 1 ppm.

X-ray absorption spectroscopy (XAS) and Mössbauer spectroscopy data collection and analysis

Samples for Fe XAS and Mössbauer spectroscopy analysis were prepared by equilibrating activated nontronite suspensions with aqueous As(III) at pH 6.0±0.5, with pH adjusted by adding dilute hydrochloric acid or sodium hydroxide. Arsenic concentration in the reactors was 1 mM, and the 47 mM As(III) stock solution was prepared from sodium arsenite $NaAsO_2$. The background electrolyte in all experiments was 0.01M sodium chloride. To terminate the reaction, clay mineral suspensions were centrifuged, and solids were separated in an anaerobic glove box.

For XAS analysis, solids were stored in liquid nitrogen atmosphere. For Mössbauer analysis, solids were dried in the anaerobic glove box, and kept under anoxic conditions prior to analysis.

Extended X-ray absorption spectroscopy (XAFS) data at the iron K-edge was collected at the Advanced Photon Source (APS), at Argonne National Laboratory at the beamline 20-ID (XOR). The beamline is equipped with a Si(111) monochromator. An uncollimated X-ray beam was used and the monochromator was detuned by 15%. The monochromator was calibrated using iron metal reference foil at the Fe K-edge at 7,112 eV. The monochromator step size was 10 eV in the pre-edge, 0.5 eV in the XANES region, and 0.05 $Å^{-1}$ in the XAFS region. Fluorescent counts were collected using a Vortex Si Drift solid state 4 element detector. The samples were kept at 22 K (-250 ºC) temperature, using a Displex liquid helium cryostat to avoid X-ray beam-induced redox transformations. Standards for Fe(III) and Fe(II) were iron (III) oxide Fe_2O_3, and iron (II) sulfate $FeSO_4$. To avoid sample oxidation during sample transport to the beamline they were kept in a dry shipper (N_2 atmosphere, liquid N_2 temperature).

The XAS data processing was done using the Athena interface, and the fitting of XAFS data was done using the Artemis interface [31] to the IFEFFIT [32] program. The background subtraction (AUTOBK algorithm [33]), normalization and conversion into k-space was conducted as described elsewhere.[34] The Fourier-transformed Fe K-edge XAFS spectra were analyzed using the Artemis interface to Ifeffit by fitting theoretical paths[35] based on the structure of nontronite. The fitting was done in R-space using a Kaiser-Bessel window and k-weights of 1, 2, and 3. The amplitude reduction factor (S_0) was determined from fitting Fe_2O_3 XAFS spectra.

Mössbauer spectroscopy data was collected using a WissEl Elektronik (Germany) instrument that included a closed-cycle cryostat SHI-850 obtained from Janis Research Co., Inc. (Wilmington, MA), a Sumitomo CKW-21 He compressor unit, and an Ar-Kr proportional counter detector (LND, Inc. NY). A ^{57}Co/Rh source (50-mCi to 75-mCi, initial strength) was used as the gamma energy source. The transmitted counts were stored in a multichannel scalar (MCS) as a function of the energy (transducer velocity) using a 1024-channel analyzer. The raw data were folded to 512 channels to provide a flat background and a zero-velocity position corresponding to the center shift (CS) of a metal Fe foil at room temperature (RT). Calibration spectra were obtained with a 20-μm-thick Fe foil placed in the same position as the samples to minimize any geometry errors. The Mössbauer spectroscopy data was modeled with Recoil software (University of Ottawa, Canada) using a Voigt-based structural fitting routine.[36] The sample preparation was identical to the procedures reported in Peretyazhko et al. (2012).[37]

Diffuse reflectance spectroscopy

Samples for diffuse reflectance measurements were prepared in several batch reactors, summarized in Table 1. We (1) compared spectral features of the native and activated nontronites NAu-1; (2) tested how the addition of varying concentrations of Fe^{2+} affects the spectral features of native nontronite NAu-1 (Supporting Information (SI)); and (3) recorded the evolution of the DR spectra following the addition of As(III) to the suspensions with native and activated NAu-1.

Table 1. Experimental conditions for all batch reactors examined by diffuse reflectance (DR) spectroscopy. The nontronite suspension density was 2 g L^{-1} in all systems. The background electrolyte was HEPES buffer at pH 7.0.

Substrate	Reaction times, minutes	pH initial	pH final	As(III) (mM)	Fe(II) (mM)	HEPES buffer (M)
NAu-1	n/a	6.94	6.88	/	/	0.895
NAu-1	16, 61, 1452, 2853	6.90	6.95	0.01	/	0.895
NAu-1	15, 61, 1450, 2851	6.90	6.90	0.1	/	0.893
NAu-1	15, 63, 1450, 2853	6.91	6.95	1	/	0.875
NAu-1	16, 63, 1451, 2854	6.93	6.91	10	/	0.695
NAu-1	n/a	6.96	6.97	/	/	0.895
NAu-1	16, 59, 1441	6.88	6.91	/	0.01	0.895
NAu-1	17, 60, 1440	6.88	6.90	/	0.1	0.893
NAu-1	17, 60, 1441	6.94	6.86	/	1	0.875
NAu-1	15, 60, 1440	7.02	6.90	/	10	0.695
Activated NAu-1	n/a	7.03	7.04	/	/	0.901
Activated NAu-1	16, 61, 1460, 2885	7.02	7.03	0.01	/	0.901
Activated NAu-1	15, 59, 1459, 2884	7.04	7.08	0.1	/	0.899
Activated NAu-1	15, 60, 1460, 2882	7.03	7.06	1	/	0.881
Activated NAu-1	16, 60, 1460, 2881	7.01	7.04	10	/	0.701

Clay mineral suspensions containing aqueous As(III) or Fe(II) were prepared in an anaerobic glove box. The NAu-1 suspensions, and the HEPES buffer and DI water were deoxygenated by keeping the suspensions under vacuum overnight prior to placing in the glove box. All DR experiments were performed in the HEPES buffer solution at a target pH of 7.0±0.1. This pH is optimal for recording the Fe(II)↔Fe(III) intervalence charge-transfer bands, as shown in previous reports.[11] The stock solution of 1 M HEPES buffer was prepared by dissolving 23.83g of HEPES in 80 mL of DI water. Sodium hydroxide NaOH pellets were added until pH reached 7 ±0.5, then the 50 % v/v NaOH was added dropwise, until pH reached 7.0. The 50 mM aqueous Fe(II) stock solution was prepared in an anaerobic glove box by dissolving ferrous chloride $FeCl_2 \cdot 4H_2O$ in deoxygenated DI water. The 47 mM aqueous As(III) solution was prepared by dissolving sodium arsenite $NaAsO_2$ in DI water. The clay suspension density was 2 g l^{-1} in all DR experiments. The aqueous concentrations of As(III) or Fe(II) were 0.01 mM, 0.1 mM, 1 mM, and 10 mM. Following the addition of either Fe(II) or As(III), the pH was measured, and

adjusted if necessary using 50% v/v NaOH. After the addition of Fe^{2+}, samples were equilibrated under anoxic conditions for 15 minutes, 1 hour, and 24 hours, prior to collecting DR spectra. In the reactivity experiments, where aqueous As(III) was added to the native and activated NAu-1 suspensions, DR measurements were performed after 15 minutes, 1 hour, and 24 hours, and for some samples after 48 hours.

A USB2000 UV-vis spectrophotometer with a halogen lamp and a fiber optic probe was used to record DR spectra. The white reflectance standard used was a halon reflective standard. The Spectra Suite (Ocean Optics) software was used to obtain spectral data in the reflection mode in the 420-1,000 nm range with an integration time of 20-350 ms. Spectral data for standards and samples was an average of 20 scans (0.4-7 sec per scan), and each measurement was taken in triplicate. Spectra were taken by submerging the fiber optic probe in a vial with 10 mL of clay mineral suspension. The spectrometer and laptop were contained in the anaerobic glove box during experiments. The spectral data for standards and samples were taken in a light-blocking vessel, constructed from a brown glass bottle, additionally wrapped in aluminum foil to eliminate ambient light. Prior to data analysis, the reflectance spectra were converted to absorbance. Origin Pro 2015 was used to integrate the broad spectral peaks between 675-775 nm. The trapezoidal rule was used to integrate each of the peaks in Origin Pro. Error bars at the 99% confidence level were calculated as three times the standard deviation of the three repeated measurements.

First principles calculations

DFT+U calculations apply the VASP code version 5.3[38-41], the PBE functional,[42] a Hubbard augmentation of Fe 3d orbitals with U-J=4 eV, and impose a 400 eV energy cut-off. The

simulation cells had dimensions 32.0x18.2x9.9 A^3. A 1x1x2 *k*-point grid was used. The basic simulation cell is shown in Figure 5. The baseline system has a $Fe_{24}Si_{48}O_{163}H_{51}Na_8As$ stoichiometry, and all iron is in +3 oxidation state Fe(III), and arsenic is in +3 oxidation state As(III). By breaking apart one of the adsorbed H_2O molecules, inserting the O onto the As(III), and placing two protons on the surface, we created a cell with the same stoichiometry with As(V) and two Fe(II). The cell is always charge-neutral. Therefore, adding a H^+ leads to another Fe(III) being reduced to Fe(II). This allowed us to examine the effect of injecting Fe(II) into the system. We compared the energy changes with and without this added H^+, for simulation cells containing As(III) and As(V).

Results and Discussion

Spectroscopic investigation of iron species residing in clay mineral structures

We used X-ray absorption (XAS), and Mössbauer spectroscopies *ex situ*, and diffuse reflectance (DR) spectroscopy *in situ* to identify the reactive iron species. XAS and Mössbauer spectroscopies are sensitive to the oxidation state and the local coordination environment around iron.[13-15, 43] We examined the local molecular environment of iron in exclusively-Fe(III) nontronites, as well as in activated nontronites before and after reacting them with arsenic As(III). Activation of the nontronite surface was achieved by partial reduction treatment, when a fraction of total iron (initially, all Fe(III)) is converted to Fe(II) *via* abiotic reduction. Based on the sum of all spectroscopic data and mass balance calculations, we conclude that edge-sharing octahedral iron moieties, written here as Fe^{II}-O-Fe^{III}, at the edge sites of nontronite are the reactive species during the oxidation of As(III) to As(V) under anoxic conditions.

To quantify the oxidation state of iron, and its local chemical environment in the native and activated nontronite, we used both XAS and Mössbauer spectroscopies. Linear combination fitting of XAS data between measured Fe(II) and Fe(III) standards shows that in the native nontronite, all Fe is in a +3-oxidation state, and in the nontronite activated by partial reduction treatment, 20±10% of total Fe is Fe(II), and 80±10% is Fe(III). The XAS and Mössbauer analysis, discussed later in this section, agree.

XAS data indicates that Fe(III) resides in an octahedral site in both activated and native nontronites, based on the shape of the pre-edge line and shell-by-shell fitting. The results of the shell-by-shell fitting of the extended X-ray absorption fine structure spectroscopy (XAFS) for activated and native nontronite are summarized in Supporting Information. These results indicate that before and after the activation treatment the structure of nontronite was nearly identical: the 1st Fe-O distance is characteristic of octahedrally-coordinated iron, (2.06 ±0.01 Å), and there is no evidence for any tetrahedral Fe in the structure. The Fe-Fe backscattering at 3.10 (±0.06) Å is characteristic for the edge-sharing iron octahedra. The activation treatment resulted in a slight increase in the magnitude of the Fe-Fe backscattering shell at 3.11±0.06 Å and Fe-O shell at 3.75±0.05 Å. This likely indicates local migration of a fraction of iron atoms into di-octahedral vacancies, and forming tri-octahedral domains, as reported earlier.[13] The structure of nontronite is preserved during the activation treatment.

Mössbauer spectra were obtained for activated nontronite samples with and without prior reaction with As(III). Samples were analyzed at room temperature (RT), 150K, and 12K (Figure

2). The most notable difference between the reacted and non-reacted samples is seen in the high-energy Fe(II) doublet peak at ~ 3 mm sec^{-1} velocity.

Figure 2.

Figure 2. Variable temperature ^{57}Fe-Mössbauer spectra collected on activated nontronite NAu-1 and activated nontronite NAu-1 after it was reacted with As(III) under anoxic conditions. (a) Spectra collected at room temperature (RT), (b) spectra collected at 150 K, and (c) Spectra collected at 12 K.

Our Mössbauer results indicate that the non-activated nontronite NAu-1 is free of Fe(II), as well as devoid of Fe(III)-oxide coatings (Figure S2 in SI). Regardless of type and crystallinity, Fe(III)-oxides display sextet features at 12 K, which are absent in our data.[16, 44, 45] In high quality Mössbauer data, such as our spectra, characteristic features due to Fe(II) and Fe(III)-oxide are detectable even at 1-2% of total Fe.[24, 46] The purity of our nontronite allowed us to probe the reactivity of iron that resides in the mineral structure. Consistent with XAS analysis, Mössbauer data indicates that the activated nontronite contains some Fe(II). More importantly, Mössbauer data shows there are distinct chemical environments for Fe(II) species in the activated sample. Mössbauer spectra collected at room temperature (RT) and 12 K on activated nontronite and activated nontronite reacted with As(III) for 2 weeks are modeled (Figure 3; Table 2). These analyses were performed to: a) identify reactive Fe(III) species responsible for the oxidation of As(III) to As(V), and b) estimate the relative distribution of the various Fe species. Modeling was performed using Voight-based structural fitting routine.[36]

In the activated sample (Figure 3a), we identified two distinct Fe(II) species in the room temperature spectrum: a) a distinct Fe(II) doublet (Fe(II)-1 in Figure 3), and b) a broad doublet feature with an average center shift value intermediate of Fe(II) and Fe(III), labeled as [Fe(II)-2+Fe(III)-2] in Figure 3. The [Fe(II)-2+Fe(III)-2] species is only observed in the RT spectrum, due to fast electron hopping between Fe(II) and Fe(III) at a rate faster than the Mössbauer detection time. Theoretical study by Alexandrov et al., 2013 predicts this behavior.[46] This broad feature observed in our RT spectrum is similar to the mixed Fe(II)-Fe(III) feature in >150 K spectra, reported in earlier publications for NAu-2 nontronite reduced with aqueous Fe^{2+}, where this species was assigned to edge-site position.[25] The nature or location (edge or basal plane) of the distinct Fe(II) that is not experiencing electron hopping with neighboring Fe(III), however, is not certain. This species could be an Fe(II) center with immediate Al(III) neighbor or an Fe(II) with Fe(III) neighbor, but not undergoing electron hopping at RT, located either at edges or in the interior of the clay mineral. Inversely, Fe(II)-1 species could be located in the interior of the clay mineral, since our citrate-bicarbonate-dithionite reduction treatment has been shown to reduce iron in clay minerals pseudo-randomly. [17] Significantly higher, and easily discernable, Fe(II) signal as well as the absence of a broad [Fe(II)-2+Fe(III)-2] feature (noted in RT spectrum) in the 150 K and 12 K spectra (Figures 2 and 3b), unambiguously suggests that: a) electron hopping between the Fe(II)-2-O-Fe(III)-2 centers stops or slows down below RT, and b) the 12 K Fe(II) feature is a composite of Fe(II)-1 and Fe(II)-2 (labeled as Fe(II)-1 + Fe(II)-2 in Figure 3). Attempts to generate a fit with 2 Fe(II) doublets are not fruitful since equally good fits with varying Fe(II)-1 and Fe(II)-2 ratios are possible (see SI). Mössbauer parameters of the Fe(II) centers (either 1 doublet or 2 doublets) are similar to edge-Fe(II) produced in an aqueous Fe^{2+}-NAu-2 system;[24] edge- and basal-O-Fe(II) display significantly different Mössbauer

parameters.[24] This is intriguing, given dissimilar environments for Fe(II) when Fe^{2+}- spiked and CBD-reduced systems are compared. In a CBD-reduced mineral Fe(II) is distributed randomly through the clay mineral particles,[17] while in an Fe^{2+}-spiked system, Fe^{2+} first adsorbs onto the edge sites (*via* inner-sphere complexation), then due to interfacial electron transfer it is converted into Fe(III) at the edge site.[25] This difference in the location of Fe(II) is expected to influence edge-Fe(II) Mössbauer parameters. The precise nature of Fe(III) center(s) that are not undergoing electron hopping with neighboring Fe(II) is complex, since center shift and quadrupole splitting values are sensitive to the identity of immediate neighboring atoms (Fe, Al, Si).[18] Also, reduction affects crystal structure (see XAFS section). Therefore, an optimal fit for RT data is achieved with two doublets, Fe(III)-1 and Fe(III)-1', and for 12 K feature—with one doublet that is a composite of Fe(III)-1, Fe(III)-1', and Fe(III)-2 contributions. The lack of sextet features in the activated sample at 12 K unambiguously indicates that no dissolution of nontronite and no crystallization of other phases took place during reduction treatment. This agrees with Jaisi et al., 2008 study,[6] where clay mineral dissolution was only noted when the extent of iron reduction was greater than 30% of total.

The Mössbauer spectra of activated nontronite NAu-1 that was reacted with As(III) for 2 weeks (336 hours) is significantly different, compared to unreacted counterpart (Figure 3). After reaction with As(III), we observe lower content of [Fe(II)-2+-Fe(III)-2] with concurrent increase in Fe(II)-1 amounts in its RT spectrum and total Fe(II) content at 12 K. These changes suggest that Fe(III) located next to Fe(II) at edge sites is the reactive Fe(III) species. Similar, combined Fe(III)-1 + Fe(III)-1' content (at RT) in the As(III)-reacted and unreacted samples further confirms that edge-Fe(III) experiencing electron hopping with neighboring Fe(II) at RT as the

reactive species (Figure 3c). The average calculated oxidation state of activated nontronite decreased from 2.23 to 2.06, following the reaction with As(III) for 2 weeks (See SI Table S2 and footnotes). The mass-balance derived average Fe oxidation states are qualitatively in agreement with the derived center shift (CS) values. The CS value of the As(III)-reacted sample is lower than for the non-reacted one. This result further reveals that Fe(III) in the Fe(II)-2+Fe(III)-2 domain at edge site (Fe^{II}-O-Fe^{III} moieties) is responsible for the oxidation of As(III). Furthermore, negatively charged AsO_3^{3-} species are expected to have a greater preference to edge sites than to negatively charged basal planes.

Figure 3.

Figure 3. Comparison of ^{57}Fe-Mössbauer spectra of activated nontronite collected at room temperature (RT) (a) and at 12 K (b) and activated nontronite after it was reacted with As(III) for 2 weeks (c, d). Selected components are shown (colored lines) together with the overall fit (black line). The summary of fitting in shown in Table 2.

Table 2. Modeled Mössbauer spectral parameters. The contributions from the identified Fe species to the overall Mössbauer spectra are shown in Figure 3.

Sample	Temp. K	HWHM[1] (mm s^{-1})	Phase	<CS>[2] (mm s^{-1})	<Δ>[3] (mm s^{-1})	σ_Δ[4] (mm s^{-1})	phase %[5]	$\chi^{2,6}$
Activated NAu-1	273	0.15	Fe(II)-1	1.2	2.51	0.34	12.43(78)	2.3
			Fe(III)-1	0.49	0.37	9e-5	9.3(24)	
			Fe(III)-1’	0.39	0.5	0.25	60.2(24)	
			Fe(II)-2+Fe(III)-2	0.81	1.17	0.78	18.0(20)	
Activated NAu-1	12	0.18	Fe(II)-1+Fe(II)-2	1.24	2.92	0.15	26.33 (24)	1.2
			Fe(III)-1+1’+2	0.5	0.53	0.25	73.67 (24)	
Activated NAu-1+ As (III), 2 weeks	273	0.18	Fe(II)-1	1.19	2.59	0.32	18.53(95)	1.2
			Fe(III)-1	0.53	0.33	0.053	10.0(30)	
			Fe(III)-1’	0.4	0.51	0.24	59.6(24)	
			Fe(II)-2+Fe(III)-2	0.86	1.24	0.71	11.88(91)	

Activated NAu-1+ As (III), 2 weeks	12 K	0.23	Fe(II)-1+Fe(II)-2 Fe(III)-1+1'+2	1.25 0.51	2.92 0.52	0.1 0.22	29.71(20) 70.29(20)	2.1

Notes:
[1] Lorentzian half-width at half-maximum
[2] center shift
[3] quadrupole splitting
[4] std dev of Δ
[5]% total Fe (2σ std dev)
[6]goodness of fit

The post-reaction examination of samples by Mössbauer spectroscopy indicates that Fe^{II}-O-Fe^{III} moiety is the redox-active species when nontronite is reacted with aqueous arsenic As(III) under anoxic conditions. We used diffuse reflectance (DR) spectroscopy to track the Fe^{II}-O-Fe^{III} species *in situ*, in clay mineral suspensions. Activated nontronite was tested with and without reacting it with As(III). Identical to the XAS and Mössbauer investigations, activation was achieved by partial reduction treatment. As quantified by Mössbauer spectroscopy, the amount of Fe(II) in the activated NAu-1 was 10.4% of Fe(total). In our previous work we demonstrated that besides partial reduction, activation of nontronite surface may also be achieved by the addition of aqueous Fe^{2+}, which adsorbs onto the nontronite surface.[28]

In the DR spectra we observed the Fe(II)↔Fe(III) intervalence electron transfer band [11] in the nontronite samples that contained Fe(II). A broad peak was centered around 720 nm and was seen exclusively in nontronite suspensions where Fe(II) was present. This spectral feature arises due to rapid electron hopping between Fe(II) and Fe(III) adjacent to each other in clay mineral structures.[11] The XAS and Mössbauer data show that the edge-sharing iron-iron moieties exist in nontronite, and these moieties in activated nontronite can contain Fe(III)+Fe(III), and

Fe(II)+Fe(III) sets. Therefore, we used this DR spectral feature to track the Fe^{II}-O-Fe^{III} moieties in real time, and *in situ*, as nontronite suspension is reacted with arsenic.

The DR spectra collected on the native and activated nontronites are shown in Figure 4. To characterize an increase or decrease in the fraction of Fe^{II}-O-Fe^{III} species, we integrated the area under the 720-nm peak, using a fixed interval between 675-775 nm. The rise of the Fe(II)↔Fe(III) intervalence electron transfer feature is observed in the activated substrates. No spectral feature was observed in the native nontronite NAu-1 suspension, consistent with the fact that this clay mineral contains exclusively Fe(III). No peak was observed for non-activated nontronite NAu-1 reacted with 10 mM As(III) under anoxic conditions, consistent with the earlier experimental work showing that no electron transfer takes place between As(III) and Fe(III) in native NAu-1 nontronite.[8]

In agreement with Mössbauer data, the activated nontronite NAu-1 before and after its reaction with As(III) has a broad peak at about 720 nm, indicating the presence of Fe^{II}-O-Fe^{III} domains. The peaks for activated nontronite reacted with different concentrations of As(III) have smaller areas, and the areas further decrease with time (Figure 4), compared to the activated NAu-1 not reacted with As(III). This indicates electron transfer between As(III) and Fe^{II}-O-Fe^{III} moieties in the clay mineral structure, and that Fe^{II}-O-Fe^{III} moieties are consumed during the reaction with As(III). The proposed reaction is:

$$[Fe^{II}\text{-O-}Fe^{III}\text{-O-}Fe^{III}] + H_3AsO_3 + H_2O \rightarrow [Fe^{II}\text{-O-}Fe^{II}\text{-O-}Fe^{II}] + H_3AsO_4 + 2H^+ \quad \text{(R1)}$$

Iron shown in square brackets indicates tri-octahedral domains in clay mineral structure.

Figure 4.

Figure 4. Diffuse reflectance (DR) data; (a) DR spectra for native and activated nontronite NAu-1, showing Fe(II)↔Fe(III) intervalence electron transfer peak in activated nontronite, centered around 720 nm; (b) Integrated area (between 675-775 nm) for native and activated nontronite NAu-1 reacted with As(III), spectra collected after 15 minutes of reaction, and As(III) concentrations were 0, 0.01mM, 0.1mM, 1mM, and 10 mM; (c) Changes in the integrated area of the Fe(II)↔Fe(III) intervalence electron transfer peak with reaction progress (the concentration of As(III) was 1 mM). Errors at 99% confidence level are shown.

We calculated electron balance, based on our earlier work on the oxidation of As(III) to As(V) on NAu-1 surface.[8, 28] We observed ~ 20% oxidation of As(III) to As(V) in the activated NAu-1 suspensions with 5 g L^{-1} density, where initial concentration of As(III) was 0.02 mM. The total iron content of the 100-mL reactors is 2.17 mmoles, and the total arsenic content is 0.002 mmoles (> 1,000-fold excess). Given the ratio of basal to edge surface area in clay minerals is on the order of 18-30%,[47] we can estimate that there was ~217 μmoles of Fe total available at the edge sites, with ~21.7 μmoles (10%) being Fe(II). We observed that only ~0.4 μmoles of As(III) was oxidized to As(V), or ~0.8 μmoles of electrons was transferred from As(III) to Fe(III) in clay mineral structure (reaction R1). This indicates, that not all Fe(III) at the edge sites was reactive, and we estimate that only 0.4% of Fe(III) available at the edge surfaces participated in the electron transfer reaction. This limited oxidation indicates that bulk Fe(III) atoms are not reactive in these systems, since even with >1,000-fold excess of Fe(III), compared to As(III), the oxidation is incomplete.

We propose that similar mechanism may be at play when As(III) is oxidized by the surfaces of iron oxides, activated by the addition of aqueous Fe^{2+}. When aqueous Fe^{2+} is added to goethite α-

FeO(OH) and lepidocrocite γ-FeO(OH) suspensions under anoxic conditions, As(III) is oxidized to As(V) by the activated surfaces.[48, 49] For these Fe(II)-activated goethite and lepidocrocite systems an intermediate reactive Fe(III) phase was proposed to form; however, this phase was not identified or characterized in the previous work. We propose that edge-sharing Fe^{II}-O-Fe^{III} moieties in these iron oxide minerals may be the reactive species, like the ones we show to be reactive in our experiments.

A proposed mechanism for the activation of Fe(III) in the presence of Fe(II) in the structure of nontronites

We conducted density functional theory with Hubbard augmentation[50] (DFT+U) calculations to estimate the energetics of electron transfer from As(III) to Fe(III)-containing nontronite with and without Fe(II) in the structure. The baseline system has a $Fe_{24}Si_{48}O_{163}H_{51}Na_8As$ stoichiometry, where initially all iron in nontronite structure is Fe(III) and arsenic is present in a +3-oxidation state. By breaking apart one of the adsorbed H_2O molecules, inserting the OH^- onto the As(III), and placing the proton on the surface, we create a cell with the same stoichiometry, but with arsenic in a +5 oxidation state. Simultaneously, two irons in clay mineral structure become Fe(II). To preserve charge neutrality, addition of H^+ leads to Fe(III) reduction to Fe(II), which allows us to examine the effect of injecting Fe(II) into the system. We found that the most favorable proton-accepting oxygen site is at a Si-O-Fe(III) bridge. We compare the energy changes with and without this added H^+, for simulation cells containing As(III) and As(V). Comparing these energies reveals the impact of Fe(II) in clay mineral structure on As(III) oxidation to As(V) on the nontronite surface.

Based on the tabulated standard redox potentials for Fe(II)/Fe(III) and As(III)/As(V) redox couples, As(III) oxidation to As(V) is exothermic in concert with Fe(III) reduction to Fe(II) in Fe-containing phyllosilicates.[8] When the simulation cell initially contains only Fe(III) (Figure 5a), the oxidation of As(III) to As(V) is slightly exothermic, with the calculated energy change of -0.05 eV. Two irons in +3 oxidation states are reduced in the process (Figure 5b). The magnitude of this energy change is not significant, because we have omitted the liquid-state water environment solvating both the nontronite edge surface and both As(III) and As(V) species. However, comparing this energy change with that in the simulation cells with one added H^+ and an electron is relevant, because there are only small local changes around that newly protonated site and a single pre-existing Fe(II). Figure 5c depicts the newly added proton and the Fe(II) formed nearby. The Si-OH-Fe configuration at the surface is more favorable, compared to other proton-accepting sites, e.g., on an existing OH-, by about 0.2 eV. In Figure 5d, the As(III) is oxidized in a way analogous to that shown in Figure 5b. With the H^+/Fe(II) pair injected, the energy associated with the oxidation of As(III) to As(V) is now +0.22 eV. Comparing with the case with exclusively-Fe(III) mineral, the oxidation of As(III) by the structural Fe(III) is less energetically favorable. In other words, Fe(II) does not make As(III) oxidation more energetically favorable. Thus, purely static thermodynamic considerations do not explain why the presence of Fe(II) "activates" nontronite surface and promotes As(III) oxidation to As(V).

To explain why Fe(II) activates nontronite surface, we propose the following possible mechanism based purely on kinetic considerations. Since arsenite AsO_3^{3-} oxidation requires it first to form an inner-sphere complex at the edge site of nontronite,[28] it must first replace surface ligands, such as H_2O. Therefore, a reduced H_2O desorption energy from the nontronite edge site

may greatly accelerate the kinetics of As(III) oxidation to As(V). When no Fe(II) is present, all adsorbed H_2O molecules are coordinated to Fe(III) (Figure 5a). When an excess H^+ and Fe(II) pair is present, they appear to preferentially exist at the nontronite edge surface. This surface Fe(II), which should facilitate H_2O desorption, is bonded to one water molecule shown in the circle in Figure 5c.

To quantify this proposed mechanism, we examine the energy cost of removing an H_2O molecule from the edge surface of model systems with and without Fe(II). Our DFT calculations indeed predict desorption energies of 0.87 and 1.18 eV, respectively, for the circled H_2O in Figures 5a and 5c. At room temperature, assuming the desorption barriers and energies are the same, the water desorption rates would be one event per 6 minutes and per 18000 hours, respectively. The presence of the liquid water environment should increase these rates, but this large difference in rates should be qualitatively preserved. Once a water molecule desorbs, an active edge site is created at which As(III) adsorption should be accelerated. While these calculations are performed for 0 K temperature and in ultra-high vacuum simulation cells, desorption energetics and H_2O desorption time scales at liquid-solid interfaces are clearly correlated.

To make the rate comparison quantitative, one should also compare the desorption rate of the reactant and product—As(III) and (As(V) oxyanions—on the nontronite surface. For these charged species, however, desorption energy barriers are likely poorly represented unless computationally costly DFT-based molecular dynamics simulations with explicit liquid water environment are conducted.[51] Such simulations will be deferred to future work. Here we

conjecture that the As(V) product will also be more weakly bound to a nontronite surface with more Fe(II) ("activated" samples) due to weaker electrostatic interactions and will desorb faster (compared to As(III)), which will lead to faster overall oxidation rate than on non-activated, Fe(III)-dominated surfaces.

We stress that this is a purely kinetic argument. The complex equilibrium partitioning of adsorbed water, As(III), and As(V) on nontronite surface, may also be slightly modified by the surface Fe(II)/Fe(III) ratio, but these equilibrium constants are not directly related to desorption rates. Note also that water desorption rates strongly depend on material and crystallographic properties of the surface. Experimental quantification of water exchange rates on Fe(II)/Fe(III) and Fe(III)-only clay minerals, as well as kinetics of inner-sphere complex formation are beyond the scope of this study. Future studies should provide experimental validation for the theoretical mechanism proposed here.

Figure 5.

Figure 5. Model nontronite edge surface with adsorbed arsenic. Adsorbed As(III) as $[AsO_2(OH)]^{2-}$ with two coordinating H_2O molecules; (b) oxidation of As(III) to As(V) (as $[AsO_3(OH)]^{2-}$ with coordinating H_2O and concomitant reduction of two Fe(III) ions to Fe(II) in nontronite structure. (c) Same as (a), but with a proton added and an Fe(III) reduced to Fe(II); (d) same as (b), but with a proton added and one more Fe(III) reduced to Fe(II). Panel (c) represents the Fe^{II}-O-Fe^{III} moiety. In panels (a) and (c), the H_2O to be removed is circled in black. Octahedra are truncated whenever Fe-O distances exceed 2.3 Å. Brown, yellow, blue, grey, red, and white depict Fe, As, Si, Na, O, and H atoms.

Summary

The redox-reactivity of Fe(III) residing in clay mineral structures is dramatically increased, following an introduction of Fe(II). This redox-activation of clay mineral surfaces can be

achieved by either partial reduction, or by the addition of aqueous Fe^{2+}, which adsorbs onto clay mineral edge sites. Once Fe(III) in clay mineral structure is "switched on", the activated nontronites oxidize As(III) *via* catalytic (oxic conditions) and, to a lesser degree, *via* direct (anoxic conditions) pathways. Here we show that Fe^{II}-O-Fe^{III} reactive moieties at the edge sites of nontronites oxidize As(III) to As(V) under oxygen-free conditions. The proposed reactive sites capable of two-electron transfer reaction for the oxidation of As(III) to As(V) are shown in Figure 6. In our earlier work we show that even with 1,000-fold excess of Fe(III), compared to As(III), we only observe partial oxidation of As(III) in these systems. This macroscopic observation strongly points to the fact that the number of reactive Fe(III) sites is limited, with only a fraction of structural Fe(III) in nontronites being accessible for redox transformations. This indicates that only edge surface sites participate in the reaction. The formation of an inner-sphere adsorption complex is a necessary step for the redox transformation *via* catalytic and direct oxidation pathways. In order for an inner-sphere complex to form, water molecules need to desorbed from the edge site. The binding energy of a water molecule at an Fe(II)-containing edge surface site is significantly lower compared to the same site, but with iron being Fe(III). We propose that this lower barrier for the desorption of water at the edge sites increases the apparent kinetics of redox reactions on clay mineral surfaces. This improved fundamental understanding of the Fe(II)/Fe(III) redox couple reactivity can be used to design reactive adsorbents and membranes, and predict environmental fate and transport of redox-sensitive chemical species.

Figure 6.

Figure 6. Proposed reactive sites for the oxidation of As(III) to As(V). Depicted is octahedral sheet of nontronite NAu-1 (we omitted tetrahedral sheet and hydrogen atoms for clarity). We propose that Fe^{II}-O-Fe^{III} moieties at the mineral edges are the reactive sites. Since two electrons

have to be transferred from As(III) to Fe(III), in order to oxidize As(III) to As(V), we propose two possible scenarios: (a) when As(III) is adsorbed to one Fe(III) and one Fe(II), both of which share an edge with another Fe(III); and (b) when As(III) is adsorbed to two Fe(III) ions in the structure, both of which are in the edge-sharing configuration with another Fe(II).

Author contributions

AGI led the project and experiment development, collected and analyzed X-ray absorption spectroscopy data. RKK collected and analyzed Mössbauer data. KL constructed computational models and interpreted DFT results. REW collected diffuse reflectance data and analyzed it together with AGI. All authors have contributed to writing and approved the final version of the manuscript.

Acknowledgements

This material is based upon work supported by the U.S. Department of Energy, Office of Science, Office of Basic Energy Sciences, Chemical Sciences, Geosciences, and Biosciences Division. Sandia National Laboratories is a multimission laboratory managed and operated by National Technology and Engineering Solutions of Sandia, LLC., a wholly owned subsidiary of Honeywell International, Inc., for the U.S. Department of Energy's National Nuclear Security Administration under contract DE-NA-0003525. Mössbauer measurements and data analysis were performed at Environmental Molecular Sciences Laboratory, a DOE Office of Science User Facility sponsored by the Office of Biological and Environmental Research and located at Pacific Northwest National Laboratory. X-ray Absorption Spectroscopy experiments were performed at the Sector 20 at Advanced Photon Source, an Office of Science User Facility operated for the U.S. Department of Energy (DOE) Office of Science by Argonne National Laboratory, and was supported by the U.S. DOE under Contract No. DE-AC02-06CH11357, and

the Canadian Light Source and its funding partners. We thank Dr. Chengjun Sun for help during data collection, and Brandon M. Ilgen for editorial comments on this manuscript.

Disclaimer

This paper describes objective technical results and analysis. Any subjective views or opinions that might be expressed in the paper do not necessarily represent the views of the U.S. Department of Energy or the United States Government.

Competing interests

The authors declare no competing interests.

Materials & Correspondence

Correspondence and material requests should be addressed to A.G. Ilgen.

Data availability

All data generated or analyzed during this study are included in this published article (and its Supplementary Information files).

Supplementary Information

Supplementary Information contains parameters from shell-by-shell fitting of X-ray absorption spectroscopy data, parameters for Mössbauer data analysis, and details on diffuse reflectance spectroscopy method development.

References

1. F. Bergaya and G. Lagaly, in *Handbook of Clay Science*, eds. F. Bergaya and G. Lagaly, Elsevier, Amsterdam, the Netherlands, 2006, vol. 1, ch. 1, pp. 1-18.
2. J. Stucki, in *Handbook of Clay Science*, eds. B. F. and L. G., Elsevier, Amsterdam, the Netherlands, 2 edn., 2013, vol. 5A, ch. 11, pp. 423–475.
3. A. Neumann, M. Sander and T. Hofstetter, in *Aquatic Redox Chemistry*, eds. P. Tratnyek, T. Grundl and S. Haderlein, American Chemical Society, Washington, DC, 2011, ch. 17, pp. 361-379.
4. T. Hofstetter, R. Schwarzenbach and S. Haderlein, Reactivity of Fe (II) species associated with clay minerals, *Environ. Sci. Technol.*, 2003, **37**, 519-528.
5. T. Peretyazhko, J. Zachara, S. Heald, B. Jeon, R. Kukkadapu, C. Liu, D. Moore and C. Resch, Heterogeneous reduction of Tc(VII) by Fe(II) at the solid–water interface, *Geochim. Cosmochim. Acta*, 2009, **72**, 1521-1539.
6. D. P. Jaisi, H. Dong and J. P. Morton, Partitioning of Fe (II) in reduced nontronite (NAu-2) to reactive sites: Reactivity in terms of Tc (VII) reduction, *Clays Clay Miner.*, 2008, **56**, 175-189.
7. M. Brigatti, G. Franchini, C. Lugli, L. Medici, L. Poppi and E. Turci, Interaction between aqueous chromium solutions and layer silicates, *Appl. Geochem.*, 2000, **15**, 1307-1316.
8. A. Ilgen, A. Foster and T. Trainor, Role of structural Fe in nontronite NAu-1 and dissolved Fe(II) in redox transformations of arsenic and antimony, *Geochim. Cosmochim. Acta*, 2012, **94**, 128-145.
9. M. Tong, S. Yuan, S. Ma, M. Jin, D. Liu, D. Cheng, X. Liu, Y. Gan and Y. Wang, Production of abundant hydroxyl radicals from oxygenation of subsurface sediments, *Environ. Sci. Technol.*, 2015, **50**, 214-221.
10. S. Yuan, X. Liu, W. Liao, P. Zhang, X. Wang and M. Tong, Mechanisms of electron transfer from structrual Fe (II) in reduced nontronite to oxygen for production of hydroxyl radicals, *Geochim. Cosmochim. Acta*, 2018, **223**, 422-436.
11. R. B. Merola, E. D. Fournier and M. M. McGuire, Spectroscopic investigations of Fe2+ complexation on nontronite clay, *Langmuir*, 2007, **23**, 1223-1226.
12. A. Manceau, V. Drits, B. Lanson, D. Chateigner, J. Wu, D. Huo, W. Gates and J. Stucki, Oxidation-reduction mechanism of iron in dioctahedral smectites: II. Crystal chemistry of reduced Garfield nontronite, *Am. Mineral.*, 2000, **85**, 153-172.
13. A. Manceau, B. Lanson, V. Drits, D. Chateigner, W. Gates, J. Wu, D. Huo and J. Stucki, Oxidation-reduction mechanism of iron in dioctahedral smectites: I. Crystal chemistry of oxidized reference nontronites, *Am. Mineral.*, 2000, **85**, 133-152.
14. W. Gates, P. Slade, A. Manceau and B. Lanson, Site occupancies by iron in nontronites, *Clays Clay Miner.*, 2002, **50**, 223-239.
15. A. G. Ilgen, R. K. Kukkadapu, D. DR, K. Artyushkova, C. C. JM, K. JN, J. MT, S. Chengjun, A. JM and W. RE, Synthesis and characterization of redox-active ferric nontronite, *Chem. Geol.*, 2017, **470**, 1-12.
16. E. Murad and J. Cashion, *Mössbauer spectroscopy of environmental materials and their industrial utilization*, Springer Science & Business Media, 2004.
17. F. R. Ribeiro, J. D. Fabris, J. E. Kostka, P. Komadel and J. W. Stucki, Comparisons of structural iron reduction in smectites by bacteria and dithionite: II. A variable-temperature Mössbauer spectroscopic study of Garfield nontronite, *Pure Appl. Chem.*, 2009, **81**, 1499-1509.

18. J. Cashion, W. Gates and G. Riley, Origin of the two quadrupole doublets in Nu-1 nontronite, *Journal of Physics: Conference Series* 2010, **217**, 012065.
19. C. A. Gorski, L. E. Klüpfel, A. Voegelin, M. Sander and T. B. Hofstetter, Redox properties of structural Fe in clay minerals: 3. Relationships between smectite redox and structural properties, *Environ. Sci. Technol.*, 2013, **47**, 13477-13485.
20. T. B. Hofstetter, A. Neumann and R. Schwarzenbach, Reduction of Nitroaromatic Compounds by Fe(II) Species Associated with Iron-Rich Smectites, *Environ. Sci. Technol.*, 2006, **40**, 235-242.
21. C. A. Gorski, M. Aeschbacher, D. Soltermann, A. Voegelin, B. Baeyens, M. Marques Fernandes, T. B. Hofstetter and M. Sander, Redox properties of structural Fe in clay minerals. 1. Electrochemical quantification of electron-donating and-accepting capacities of smectites, *Environ. Sci. Technol.*, 2012, **46**, 9360-9368.
22. C. A. Gorski, L. Klüpfel, A. Voegelin, M. Sander and T. B. Hofstetter, Redox properties of structural Fe in clay minerals. 2. Electrochemical and spectroscopic characterization of electron transfer irreversibility in ferruginous smectite, SWa-1, *Environ. Sci. Technol.*, 2012, **46**, 9369-9377.
23. D. P. Jaisi, R. K. Kukkadapu, D. D. Eberl and H. Dong, Control of Fe (III) site occupancy on the rate and extent of microbial reduction of Fe (III) in nontronite, *Geochim. Cosmochim. Acta*, 2005, **69**, 5429-5440.
24. A. Neumann, T. L. Olson and M. M. Scherer, Spectroscopic evidence for Fe (II)–Fe (III) electron transfer at clay mineral edge and basal sites, *Environ. Sci. Technol.*, 2013, **47**, 6969-6977.
25. M. V. Schaefer, C. A. Gorski and M. M. Scherer, Spectroscopic evidence for interfacial Fe (II)− Fe (III) electron transfer in a clay mineral, *Environ. Sci. Technol.*, 2011, **45**, 540-545.
26. Z. Wang, Probing the importance of planar surfaces and crystal edges for electron transfer within iron-bearing clays, *RSC Advances*, 2014, **4**, 31476-31480.
27. V. Alexandrov and K. M. Rosso, Insights into the mechanism of Fe (II) adsorption and oxidation at Fe–Clay mineral surfaces from first-principles calculations, *The Journal of Physical Chemistry C*, 2013, **117**, 22880-22886.
28. A. G. Ilgen, J. N. Kruichak, K. Artyushkova, M. G. Newville and C. Sun, Redox Transformations of As and Se at the Surfaces of Natural and Synthetic Ferric Nontronites: Role of Structural and Adsorbed Fe (II), *Environmental science & technology*, 2017, **51**, 11105-11114.
29. Z. M. Chan, D. A. Kitchaev, J. N. Weker, C. Schnedermann, K. Lim, G. Ceder, W. Tumas, M. F. Toney and D. G. J. P. o. t. N. A. o. S. Nocera, Electrochemical trapping of metastable Mn3+ ions for activation of MnO2 oxygen evolution catalysts, 2018, 201722235.
30. J. Stucki, D. Golden and C. Roth, Preparation and handling of dithionite-reduced smectite suspensions, *Clays Clay Miner.*, 1984, **32**, 191-197.
31. B. Ravel and M. Newville, ATHENA, ARTEMIS, HEPHAESTUS: data analysis for X-ray absorption spectroscopy using IFEFFIT, *Journal of Synchrotron Radiation*, 2005, **12**, 537-541.
32. M. Newville, IFEFFIT: interactive XAFS analysis and FEFF fitting, *Journal of Synchrotron Radiation*, 2001, **8**, 322-324.
33. M. Newville, P. Livins, Y. Yacoby, J. Rehr and E. Stern, Near-edge x-ray-absorption fine structure of Pb: A comparison of theory and experiment, *Physical Review B*, 1993, **47**, 14126-14131.
34. S. Kelly, D. Hesterberg and B. Ravel, in *Methods of Soil Analysis: Part 5--Mineralogical Methods*, eds. A. Ulery and L. Drees, Soil Science Society of America, Madison, WI, USA, 2008, ch. 14, pp. 387-465.
35. S. Zabinsky, J. Rehr, A. Ankudinov, R. Albers and M. Eller, Multiple-scattering calculations of x-ray-absorption spectra, *Physical Review B*, 1995, **52**, 2995-3009.

36. D. Rancourt and J. Ping, Voigt-based methods for arbitrary-shape static hyperfine parameter distributions in Mössbauer spectroscopy, *Nuclear Instruments and Methods in Physics Research Section B: Beam Interactions with Materials and Atoms*, 1991, **58**, 85-97.
37. T. Peretyazhko, J. M. Zachara, R. K. Kukkadapu, S. M. Heald, I. V. Kutnyakov, C. T. Resch, B. W. Arey, C. M. Wang, L. Kovarik and J. L. Phillips, Pertechnetate (TcO 4−) reduction by reactive ferrous iron forms in naturally anoxic, redox transition zone sediments from the Hanford Site, USA, *Geochim. Cosmochim. Acta*, 2012, **92**, 48-66.
38. G. Kresse and J. Furthmüller, Efficient iterative schemes for ab initio total-energy calculations using a plane-wave basis set, *Physical review B*, 1996, **54**, 11169.
39. G. Kresse and J. Furthmüller, Efficiency of ab-initio total energy calculations for metals and semiconductors using a plane-wave basis set, *Computational materials science*, 1996, **6**, 15-50.
40. G. Kresse and D. Joubert, From ultrasoft pseudopotentials to the projector augmented-wave method, *Physical Review B*, 1999, **59**, 1758.
41. J. Paier, M. Marsman and G. Kresse, Why does the B3LYP hybrid functional fail for metals?, *The Journal of chemical physics*, 2007, **127**, 024103.
42. J. P. Perdew, K. Burke and M. Ernzerhof, Generalized gradient approximation made simple, *Phys. Rev. Lett.*, 1996, **77**, 3865.
43. A. Manceau, D. Chateigner and W. Gates, Polarized EXAFS, distance-valence least-squares modeling (DVLS), and quantitative texture analysis approaches to the structural refinement of Garfield nontronite, *Phys. Chem. Miner.*, 1998, **25**, 347-365.
44. C. Chen, R. Kukkadapu and D. Sparks, Influence of Coprecipitated Organic Matter on Fe2+(aq)-Catalyzed Transformation of Ferrihydrite: Implications for Carbon Dynamics, *Environ. Sci. Technol.*, 2015, **49**, 10927-10936.
45. A. Bhattacharyya, A. Campbell, M. Tfaily, Y. Lin, R. Kukkadapu, W. Silver, P. Nico and J. Pett-Ridge, Redox Fluctuations Control the Coupled Cycling of Iron and Carbon in Tropical Forest Soils, *Environ. Sci. Technol.*, 2018, **52**, 14129-14139.
46. V. Alexandrov, A. Neumann, M. M. Scherer and K. M. Rosso, Electron exchange and conduction in nontronite from first-principles, *The Journal of Physical Chemistry C*, 2013, **117**, 2032-2040.
47. B. R. Bickmore, K. L. Nagy, P. E. Sandlin and T. S. Crater, Quantifying surface areas of clays by atomic force microscopy, *Am. Mineral.*, 2002, **87**, 780-783.
48. K. Amstaetter, T. Borch, P. Larese-Casanova and A. Kappler, Redox Transformations of Arsenic by Fe(II)-Activated Goethite (α−FeOOH), *Environ. Sci. Technol.*, 2010, **44**, 102-108.
49. L. Wang and D. E. Giammar, Effects of pH, dissolved oxygen, and aqueous ferrous iron on the adsorption of arsenic to lepidocrocite, *J. Colloid Interface Sci.*, 2015, **448**, 331-338.
50. S. Dudarev, G. Botton, S. Savrasov, C. Humphreys and A. Sutton, Electron-energy-loss spectra and the structural stability of nickel oxide: An LSDA+ U study, *Physical Review B*, 1998, **57**, 1505.
51. K. Leung and L. J. Criscenti, Lead and selenite adsorption at water–goethite interfaces from first principles, *J. Phys.: Condens. Matter*, 2017, **29**, 365101.

TOC

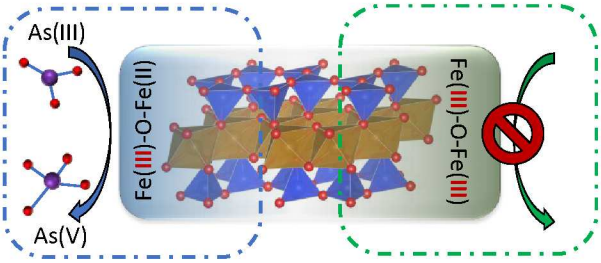

We discovered a new mechanism explaining why iron in its oxidized form Fe(III) in clay minerals is reactive only in the presence of trace amounts of its reduced form—Fe(II).

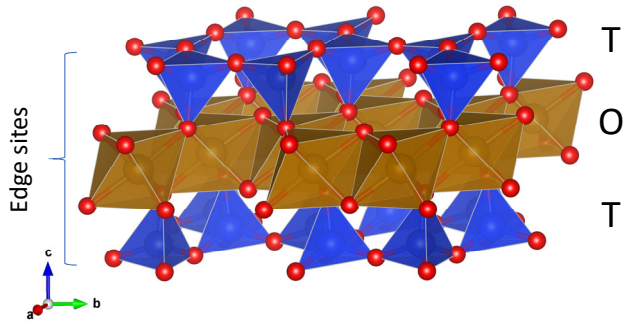
T
O
T
Edge sites
c
b
a

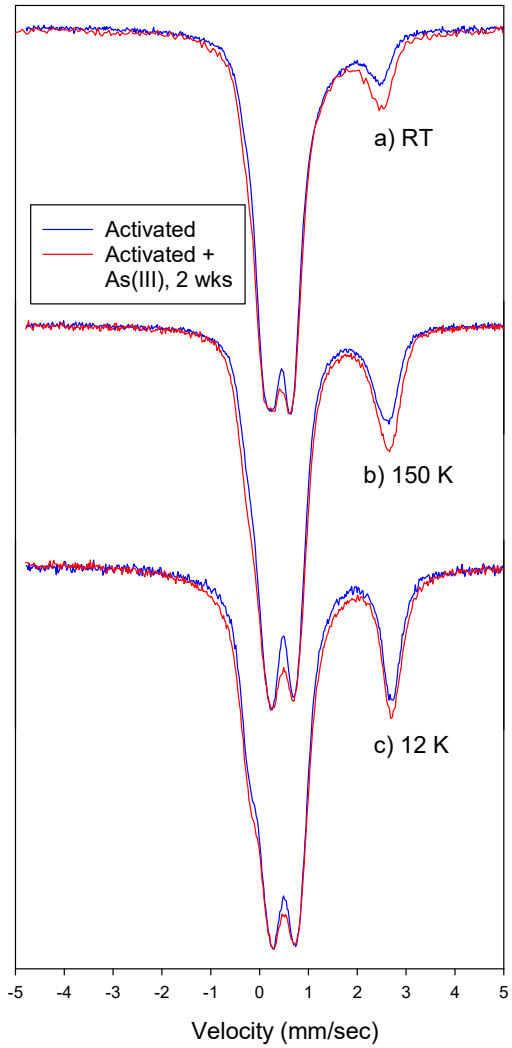
a) RT
Activated
Activated +
As(III), 2 wks
b) 150 K
c) 12 K
-5
-4
-3
-2
-1
0
1
2
3
4
5
Velocity (mm/sec)

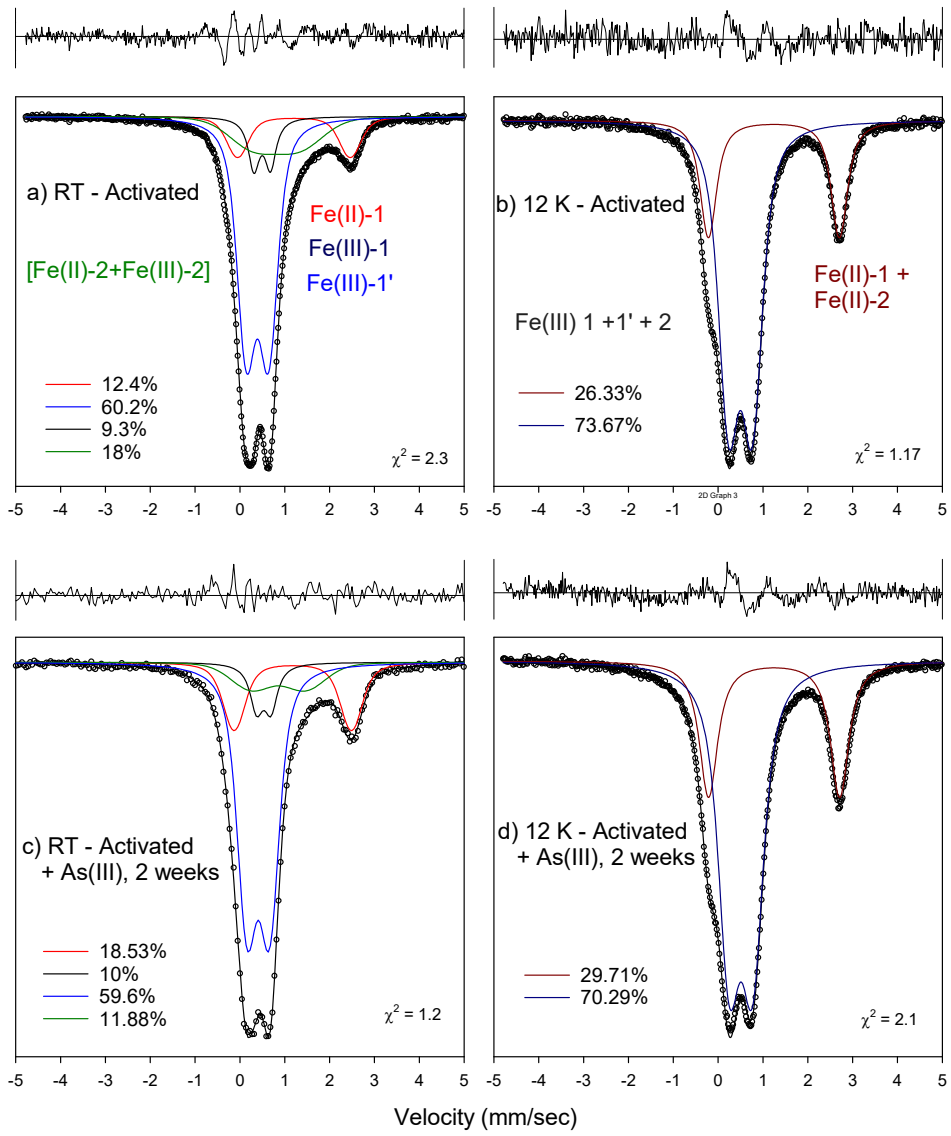
a) RT - Activated
[Fe(II)-2+Fe(III)-2]
Fe(II)-1
Fe(III)-1
Fe(III)-1'
12.4%
60.2%
9.3%
18%
χ² = 2.3
b) 12 K - Activated
Fe(III) 1 +1' + 2
Fe(II)-1 +
Fe(II)-2
26.33%
73.67%
χ² = 1.17
c) RT - Activated
+ As(III), 2 weeks
18.53%
10%
59.6%
11.88%
χ² = 1.2
d) 12 K - Activated
+ As(III), 2 weeks
29.71%
70.29%
χ² = 2.1
-5 -4 -3 -2 -1 0 1 2 3 4 5
Velocity (mm/sec)

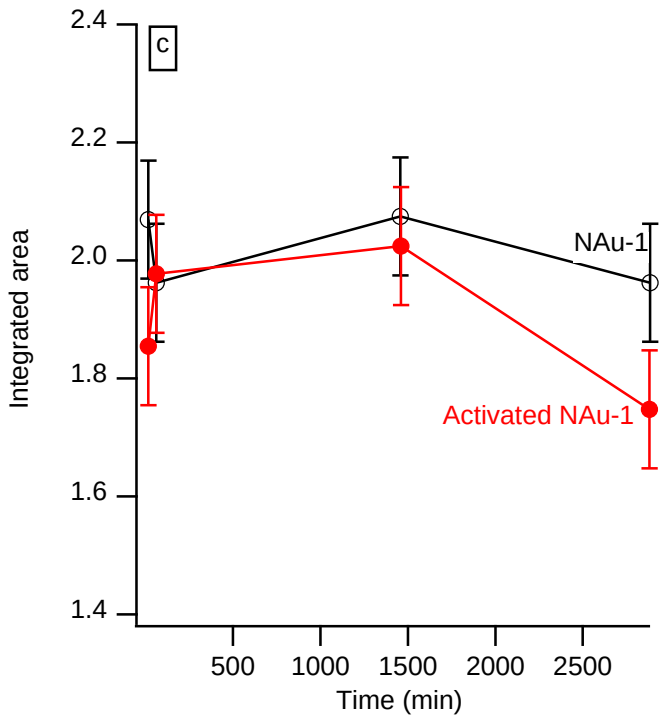
c
Integrated area
Time (min)
NAu-1
Activated NAu-1

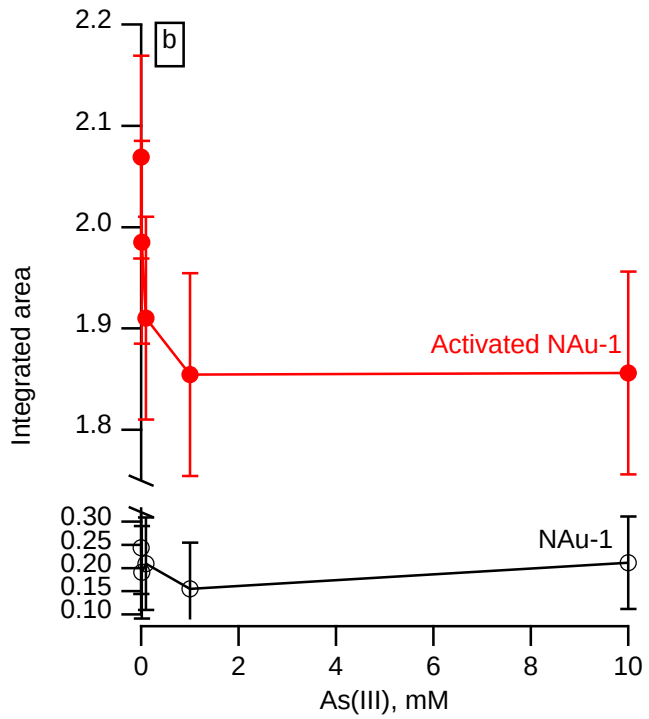
b
Integrated area
As(III), mM
Activated NAu-1
NAu-1

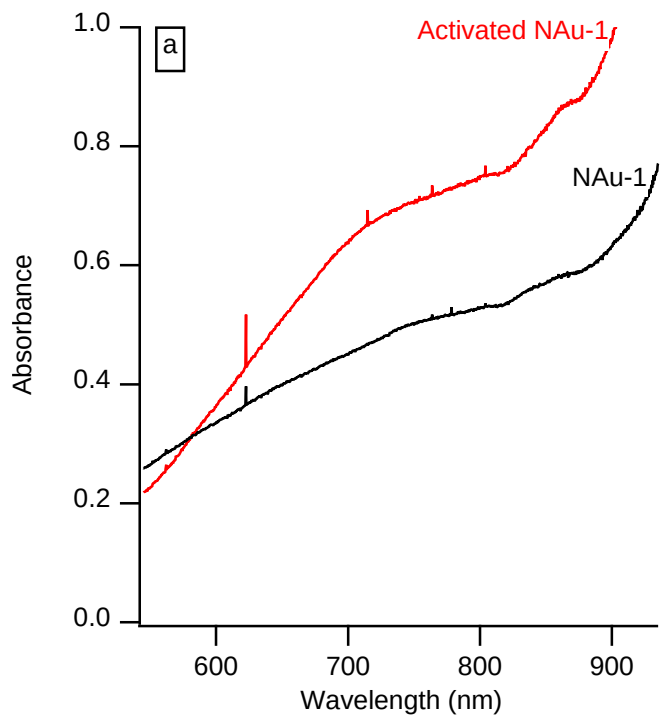
a
Absorbance
Wavelength (nm)
Activated NAu-1
NAu-1

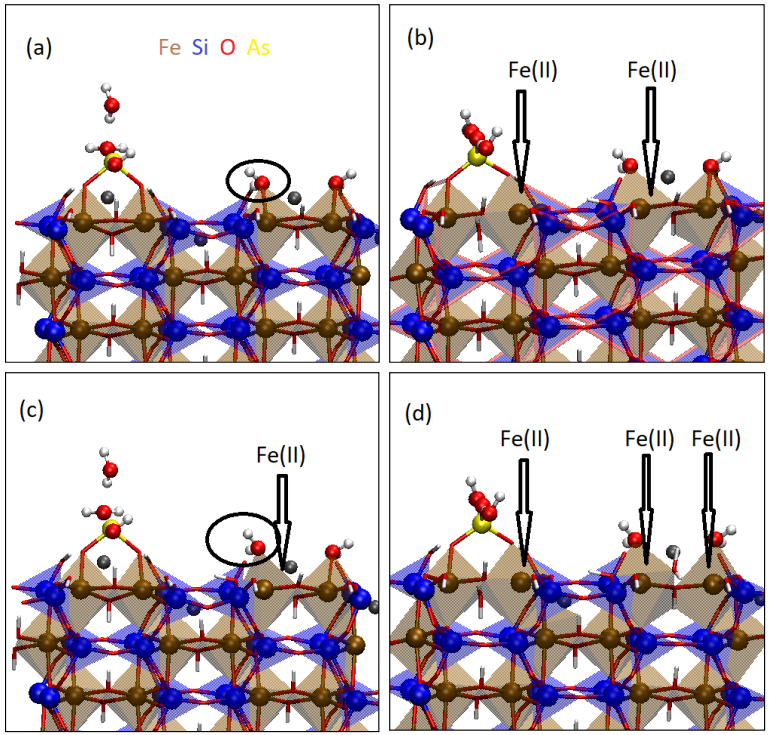
(a)
Fe Si O As
(b)
Fe(II)
Fe(II)
(c)
Fe(II)
(d)
Fe(II)
Fe(II)
Fe(II)

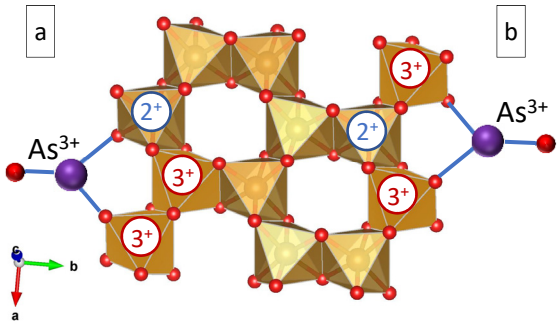
a
b
As3+
As3+
2+
2+
3+
3+
3+
3+
c
b
a